THE JOURNAL OF PHYSICAL CHEMISTRY C

Article

pubs.acs.org/JPCC

Experimental and Theoretical Studies on the Linear and Nonlinear Optical Properties of $Bi_2ZnOB_2O_6$

Xin Su,[†] Ying Wang,[†,‡] Zhihua Yang,*[,†] Xu-Chu Huang,[†] Shilie Pan,*[,†] Feng Li,[†] and Ming-Hsien Lee[§]

[†]Key Laboratory of Functional Materials and Devices for Special Environments, CAS, and Xinjiang Key Laboratory of Electronic Information Materials and Devices, Xinjiang Technical Institute of Physics & Chemistry, 40-1 South Beijing Road, Urumqi 830011, China

[‡]University of Chinese Academy of Sciences, Beijing 100049, China

[§]Department of Physics, Tamkang University, Taipei 25137, Taiwan

Supporting Information

ABSTRACT: A large single crystal of a nonlinear optical material $Bi_2ZnOB_2O_6$ (BZB) has been grown by the Czochralski method. The experiments of linear and nonlinear optical property were performed. On the basis of the density functional theory (DFT), the first-principles calculations have been employed to study the structural and electronic properties of BZB successfully. The calculated results are essentially consistent with the corresponding experimental results. In addition, to gain further insight into the structure−property relationship, a real-space atom-cutting method was adopted to analyze the origin of the nonlinear optical response of BZB for the first time. The results indicate that the contributions of the $(BiO_6)^{9-}$ and $(B_2O_5)^{4-}$ groups are dominant in the BZB crystal for producing large microscopic second-order susceptibilities.

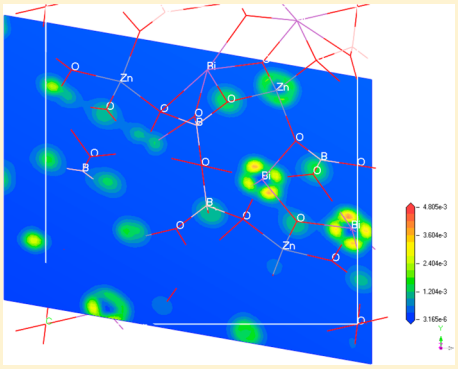

INTRODUCTION

Borate nonlinear optical (NLO) crystals have attracted considerable attention in laser science and technology due to their high resistance against laser-induced damage and high transparency in the UV region.[1−5] The discovery of the new nonlinear optical material, $Bi_2ZnB_2O_7$, was first described by Barbier et al.[6,7] in their investigation of the Bi_2O_3−ZnO−B_2O_3 system in 2005. Very recently, our group has grown large BZB crystal with high optical quality. The formula of $Bi_2ZnB_2O_7$ has been changed to $Bi_2ZnOB_2O_6$ according to its anionic structure.[8−11] Preliminary investigations of BZB indicate that it is a promising NLO material with large second-harmonic generation (SHG) response (3−4 KH_2PO_4 (KDP)), wide optical transmission range, and congruent melting property.[6−13] Considering these excellent properties of BZB, it is interesting and meaningful to grow a large single crystal and further investigate its structure−property relationship. A few theoretical studies of BZB have been published. Reshak et al. gave some results about the linear and NLO properties of BZB, but they do not calculate the SHG coefficients.[12,13] To the best of our knowledge, the mechanism of the large SHG response for BZB is still rather scarce. Therefore, a further combined experimental and theoretical study for BZB would help us to understand the origin of linear and NLO effects. In recent years, the first-principles method based on the DFT has been proved to be an effective approach for probing the structure−property relationship of many NLO materials. For example, calculations of linear and NLO properties for β-BaB_2O_4 (BBO),[4] BiB_3O_6 (BIBO),[14] LiB_3O_5 (LBO),[15] and KBe_2BO_3F (KBBF)[16] crystals have been reported with satisfactory explanations for the mechanism of NLO effects. The origins of the SHG effects for these crystals can be clearly explained by using the atom-cutting analysis method.[17] This analysis method isolates the contribution of individual atoms or clusters by removing spatial localized wave functions from the evaluation. The goal of this work is to further investigate the intrinsic correlation between the structure and the optical properties based on experimental measurements and first-principles calculations. Especially, a reasonable explanation for the origin of the optical responses will be given.

In this work, the procedure is organized as follows: first, BZB single crystal was grown by Czochralski method, and its optical transmittance spectrum, refractive-index dispersion, and the second-order optical susceptibilities were measured. Second, we have performed a computational study on the crystal structure, electronic structure, chemical bonding, and optical properties of BZB using DFT calculations with the local density approximation (LDA).[18] The calculations of electronic structure, charge density, and electron localization function (ELF) were adopted to analyze the electronic structure and optical properties of BZB. The optimizations of geometrical structures and calculations of electronic structure results are also in

Received: February 6, 2013
Revised: June 5, 2013
Published: June 5, 2013

   dx.doi.org/10.1021/jp4013448 | J. Phys. Chem. C 2013, 117, 14149−14157

agreement with the experimental ones. We believe that it will provide valuable insight into this novel class of material for their use as NLO materials. Finally, a central feature of this article is the detailed investigation of the respective contributions of subsystems to the total optical response by the real-space atom-cutting method. It is suggested that $(BiO_6)^{9-}$ and $(B_2O_5)^{4-}$ groups play important roles in the linear and NLO properties of BZB. The experimental measurements and the calculation results further indicate that BZB is a promising material for the development of solid-state laser devices applications.

EXPERIMENTAL AND CALCULATION METHODOLOGY

Experimental Details. The raw materials of BZB were prepared by solid-state reaction, with analytical purity Bi_2O_3, ZnO, and H_3BO_3 in stoichiometric proportions. Because BZB melts congruently, the Czochralski growth method was applied. Our experiments show that the molar ratio of M (Bi_2O_3)/M (ZnO)/M (H_3BO_3) = 1:1:2 is suitable to grow BZB crystals. The mixture was heated up to 800 °C, kept at that temperature for 10 h, and cooled quickly to the initial crystallization temperature of 705 °C. The seed test method was employed to measure the saturation point of the solution (about 692.5 °C). The seed crystal then was introduced into the liquid surface at a few degrees higher than the saturation point for 30 min to dissolve the outer surface of the seed crystal. The temperature was lowered quickly to saturation point, and then held at that temperature for 48 h with a seed-rotation rate of 15 rpm. When the growth of crystal ended, it was lifted out of the liquid surface and cooled to room temperature at a rate of 5 °C/h. Finally, a large BZB single crystal was obtained with an approximate size of 30 mm × 20 mm × 23 mm, which is shown in Figure 1.

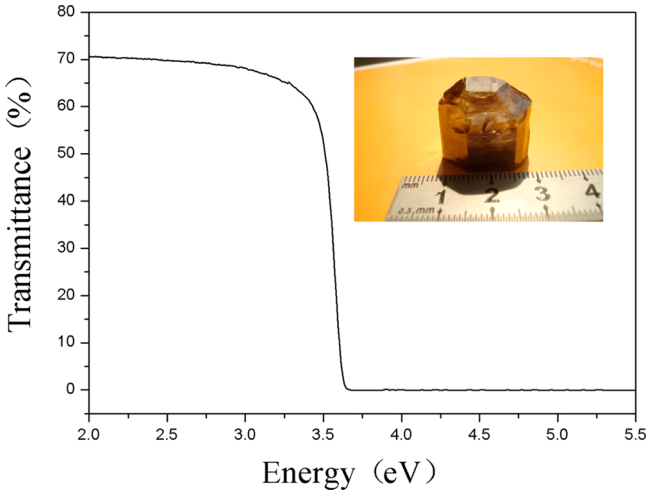

Figure 1. The photograph and transmission spectrum for BZB crystal.

The powder X-ray diffraction pattern has confirmed that the compound is a single phase (Figure S1), and the crystal data and structure refinement for BZB are given in Tables S1 and S2. Optical transmittance spectrum was measured by the Perkin-Elmer Lambda 900 UV−vis−NIR spectrophotometer in the wavelength range from 200 to 3000 nm at room temperature. As shown in Figure 1, a wide transmission range from 330 to 3000 nm is observed from the UV to IR region. An absorption edge of 360 nm and consequently an optical band gap of 3.444 eV could be deduced by the extrapolation method.[6,8] Hence, BZB is a wide-band gap semiconductor, and the wide transparency range makes the compound a potential NLO material.

The refractive-index dispersion measurements were performed by the minimum-deviation method between 400 and 1068 nm at room temperature. Because BZB belongs to the *Pba*2 space group, two prisms are needed to measure all of its refractive indices. A detailed procedure has been published.[11]

The second-order optical susceptibilities were measured via the standard Maker fringe method.[11,14,15] The morphologies and habits of BZB crystal slabs with surface orientations for three principal components (100), (010), and (001) were used in the measurements. A Q-switched Nd:YAG laser at 1064 nm with a pulse width of 10 ns and repetition frequency of 1 kHz was used as fundamental light. A (110) cut KDP slab with 2.0 mm in thickness was employed and used as the reference crystal.

Calculation Details. The experimental X-ray crystallographic data of BZB were used as the initial geometry for the theoretical calculations. The first-principles calculations are performed by the plane-wave pseudopotential method,[19−21] which employs a plane-wave basis set implemented in the CASTEP package[22] based on the DFT. The exchange correlation interaction was treated by the LDA with the Ceperley and Alder−Perdew−Zunger functional (CA-PZ). The ion−electron interactions were modeled by the optimized normal-conserving pseudopotential (NCP) for all elements,[23,24] the valence electrons were treated with a plane wave basis set, and the core electrons were handled by pseudopotential approximations.[23,25,26]

For the purpose of achieving energy convergence, a plane-wave basis set energy cutoff was 750 eV, and the Monkhorst−Pack[27] scheme was given by 3 × 3 × 6 in the irreducible Brillouin zone.[28] The chosen electronic configurations for generating pseudopotentials are Bi $5d^{10}6s^26p^3$, Zn $3d^{10}4s^{1.27}4p^{0.73}$, B $2s^22p^1$, and O $2s^22p^4$. These conditions were further applied to calculate the optical responses.

It is known that the band gap calculated by the LDA is in general smaller than the experimental data. This is due to the discontinuity of exchange-correlation energy, which will influence the accuracy of the calculated frequency-dependent response functions directly. To have the resonances occur at the correct energies, it is necessary to use a correction to the band structure. The correction is known as the "scissors" approximation and implemented by shifting all of the conduction bands with the gap correction Δ, which in all practical applications has been taken to be independent of **k** space. The scissors operator[29,30] Δ (=0.103 eV) was applied for the calculation of BZB. The momentum matrix elements should be renormalized regarding the change of the Hamiltonian in a way given by Levine and Allan[31] and later by Hughes and Sipe in a more transparent manner.[32] The associated renormalization of the momentum matrix elements under the gap correction satisfies:[18]

$$P_{nm} \rightarrow P_{nm}\frac{\omega_{nm} + \Delta/\hbar(\delta_{nc} - \delta_{mc})}{\omega_{nm}} \quad (1)$$

where the $(\delta_{nc} - \delta_{mc})$ factor restricts the gap correction to pairs of bands involving one valence and one conduction band state. An assumption that the $\mathbf{r}_{mn}$ matrix elements do not change is

dx.doi.org/10.1021/jp4013448 | J. Phys. Chem. C 2013, 117, 14149−14157

taken implicitly in this approach, because the LDA wave functions are close to the true quasiparticle wave functions.[33,34]

The calculations of linear optical properties described in terms of the complex dielectric function $\varepsilon(\omega) = \varepsilon_1(\omega) + i\varepsilon_2(\omega)$ were made. On the basis of the obtained electronic structures, the imaginary part of the dielectric function $\varepsilon_2(\omega)$ can be calculated from the electronic transition between the occupied and unoccupied states caused by the interaction with photons,[35] which is given by eq 2:[36]

$$\varepsilon_2^{ij}(\omega) = \frac{8e^2\pi^2\hbar^2}{m^2V}\sum_k\sum_{cv}(f_c - f_v)\frac{P_{cv}^i(k)P_{vc}^j(k)}{E_{vc}^2}\delta[E_c(k) - E_v(k) - \hbar\omega] \quad (2)$$

where f_c and f_v represent the Fermi distribution functions of the conduction band and valence band, respectively. The term $P_{cv}^i(k)$ denotes the momentum matrix element transition from the energy level c of the conduction band to the level v of the valence band at a certain k point in the BZ, and V is the volume of the unit cell. The symbols m, e, and $\hbar$ represent the electron mass, charge, and Plank's constant, respectively. The real part of the dielectric function is determined by a Kramers–Kronig transform.[37] The other linear optical properties such as refractive indices can be obtained accordingly.

SHG coefficients are calculated by using the so-called length-gauge formalism derived by Aversa and Sipe,[18,19] at a zero-frequency limit. The static second-order nonlinear susceptibilities $\chi_{\alpha\beta\gamma}^{(2)}$ can be reduced as:[17]

$$\chi_{\alpha\beta\gamma}^{(2)} = \chi_{\alpha\beta\gamma}^{(2)}(\mathrm{VE}) + \chi_{\alpha\beta\gamma}^{(2)}(\mathrm{VH}) + \chi_{\alpha\beta\gamma}^{(2)} \quad (\text{two bands}) \quad (3)$$

where $\chi_{\alpha\beta\gamma}^{(2)}(\mathrm{VE})$ and $\chi_{\alpha\beta\gamma}^{(2)}(\mathrm{VH})$ denote the contributions from virtual-electron and virtual-hole processes, respectively. $\chi_{\alpha\beta\gamma}^{(2)}$ (two-bands) gives the contribution from two-band processes to $\chi_{\alpha\beta\gamma}^{(2)}$. The formulas for calculating $\chi_{\alpha\beta\gamma}^{(2)}(\mathrm{VE})$, $\chi_{\alpha\beta\gamma}^{(2)}(\mathrm{VH})$, and $\chi_{\alpha\beta\gamma}^{(2)}$(two bands) are as follows:[17]

$$\chi_{\alpha\beta\gamma}^{(2)}(\mathrm{VE}) = \frac{e^3}{2\hbar m^3}\sum_{vv'c}\int\frac{d^3k}{4\pi^3}P(\alpha\beta\gamma)\,\mathrm{Im}[P_{vv'}^{\alpha}P_{cv}^{\beta}P_{cv}^{\gamma}]\left(\frac{1}{\omega_{cv}^3\omega_{v'c}^2} + \frac{2}{\omega_{vc}^4\omega_{cv'}}\right) \quad (4)$$

$$\chi_{\alpha\beta\gamma}^{(2)}(\mathrm{VH}) = \frac{e^3}{2\hbar m^3}\sum_{vcc'}\int\frac{d^3k}{4\pi^3}P(\alpha\beta\gamma)\,\mathrm{Im}[P_{cv}^{\alpha}P_{cc'}^{\beta}P_{c'v}^{\gamma}]\left(\frac{1}{\omega_{cv}^3\omega_{vc'}^2} + \frac{2}{\omega_{vc}^4\omega_{c'v}}\right) \quad (5)$$

$$\chi_{\alpha\beta\gamma}^{(2)}(\text{two bands}) = \frac{e^3}{2\hbar m^3}\sum_{vc}\int\frac{d^3k}{4\pi^3}P(\alpha\beta\gamma)\frac{\mathrm{Im}[P_{vc}^{\alpha}P_{cv}^{\beta}(P_{vv}^{\gamma} - P_{cc}^{\gamma})]}{\omega_{vc}^5} \quad (6)$$

Here, α, β, and γ are Cartesian components, v and v' denote valence bands, c and c' denote conduction bands, and $P(\alpha\beta\gamma)$ denotes full permutation. The band energy difference and momentum matrix elements are denoted as $\hbar\omega_{ij}$ and P_{ij}^{α}, respectively.

RESULTS AND DISCUSSION

A. Crystal Structure and General Characterization.

The geometric parameters of the BZB crystal are as follows: a = 10.8200(7) Å, b = 11.0014(7) Å, c = 4.8896(3) Å. As shown in Figure S2 (a), Figure S3, and Table S3, 48 atoms are presented in the primitive cell of BZB. In the structure, through sharing the O atoms, two $(BO_3)^{3-}$ triangles condense into a $(B_2O_5)^{4-}$ group (Figure S2(b)), and two $(BO_4)^{5-}$ tetrahedra condense into a $(B_2O_7)^{8-}$ group. The $(B_2O_5)^{4-}$ and $(B_2O_7)^{8-}$ groups are bridged by tetrahedral Zn^{2+} centers through sharing three O vertices of each $(ZnO_4)^{6-}$ tetrahedron, generating a two-dimensional $(ZnB_2O_7)^{6-}$ layer parallel to the (001) plane. These layers are stacked via Bi–O bonds along the crystallographic c-axis. All structural factors have their specific effects on the electronic and band structures of BZB, and, consequently, on the optical properties.

BZB crystallizes in the NCS orthorhombic space group *Pba*2, so there are three nonzero independent components of the second-order polarizability tensor, assuming the Kleinman symmetry conditions (Figure S4). The experimental measurements show that BZB is a positive biaxial optical crystal, with the dielectric axes X, Y, Z ($n^z > n^y > n^x$) corresponding to crystallographic axes b, c, a, respectively. The measured refractive indices of BZB are accurate enough to fit the Sellmeier equations of the crystal. Table S4 shows several typical wavelengths in the visible region measured and fitted refractive index data for n^x, n^y, and n^z. The Sellmeier equations of the crystal have been fitted:

$$n_x^2 = 4.05894 + 0.07743336/(\lambda^2 - 0.05031004) - 0.01020891\lambda^2 \quad (7)$$

$$n_y^2 = 4.21015 + 0.08095297/(\lambda^2 - 0.04688094) - 0.02019926\lambda^2 \quad (8)$$

$$n_z^2 = 4.37721 + 0.09408252/(\lambda^2 - 0.05175977) - 0.01752041\lambda^2 \quad (9)$$

Here, λ denotes the wavelength in micrometers. The values calculated from ours are exactly consistent with experimental ones to the fifth decimal place, which is in agreement with that in ref 11.

The phase-matching angles of BZB are calculated based on Sellmeier equations given in eqs 7–9. From Figure 2, we can see: (1) the type I phase-matching angles are $\theta = 90°$ and $\varphi = 53°$ at 1064 nm in XY plane. (2) The type I and type II phase-

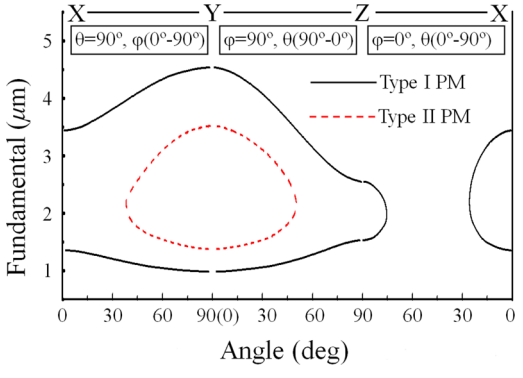

Figure 2. Phase-matching range of BZB crystal.

dx.doi.org/10.1021/jp4013448 | J. Phys. Chem. C 2013, 117, 14149–14157

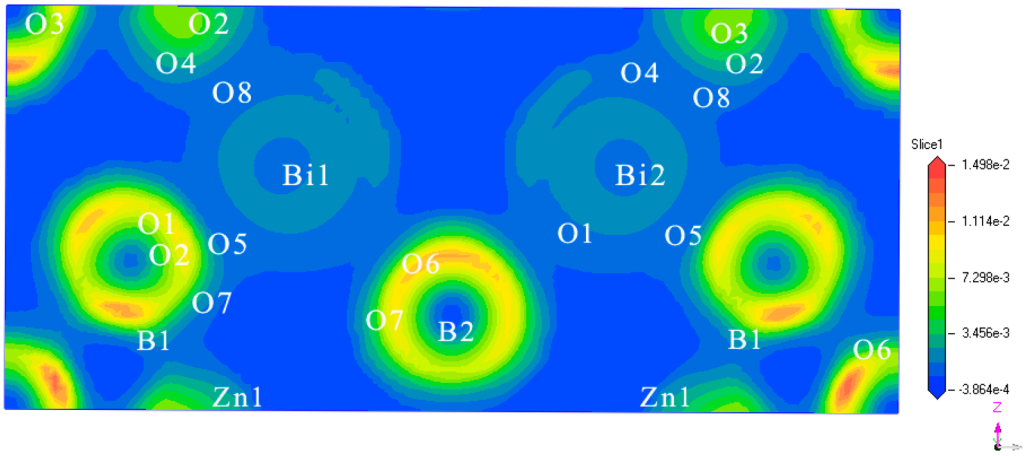

Figure 3. The plots of electronic local function (ELF) maps of BZB. The intercept direction of the plane (viewed down the *Y* axis) contains Bi1 and Bi2 atoms.

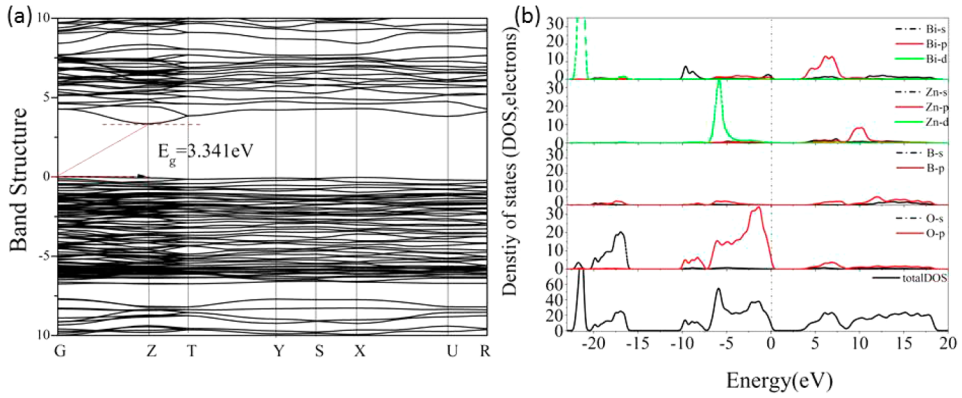

Figure 4. Band structure (a) and DOS (b) of BZB using optimized pseudopotentials.

matching SHG ranges of fundamental wavelength are from 981 to 4533 nm and from 1378 to 3513 nm, respectively. (3) BZB is type I phase matchable at 1064 nm in three principal planes (*XY*, *YZ*, *ZX*), but only type II phase matchable at 1064 nm in *XY* and *YZ* planes.

By employing the Maker fringes method, the SHG coefficients are $|d_{31}|$ = 0.911 pm/V, $|d_{32}|$ = 3.083 pm/V, and $|d_{33}|$ = 1.015 pm/V, respectively.

The effective nonlinearity $|d_{\text{eff}}^{\text{SHG}}|$ of BZB is expressed:

$$d_{32} \sin^2 \varphi + d_{31} \cos^2 \varphi \text{ (type I)} \quad (10)$$

$$d_{15} \sin^2 \theta + d_{24} \cos^2 \theta \text{ (type II)} \quad (11)$$

The $|d_{\text{eff}}^{\text{SHG}}|$ of BZB crystal for type I phase matching in *XY* plane at 1064 nm fundamental wavelength is 1.63 pm/V, which is about 4.3 times that of KDP ($|d_{\text{eff}}^{\text{SHG}}| \approx 0.38$ pm/V) and comparable to the powder SHG effect.

B. Electronic Structure. In view of the forthcoming calculations of the electronic band structure, density of states, and optical properties, it is necessary to perform an optimization of the initial crystal structure (Table S3). The optimized unit cell parameters and atomic positions are found to be close to those obtained from the experiment. To investigate the relationship between microscopic and macroscopic properties, population analyses and electron localization function (ELF) based on the electronic structures were obtained for BZB.

The Mulliken population analysis is displayed in Table S5. The calculated bond charges of Bi−O, Zn−O, and B−O bonds are 1.61−1.65, 1.04, and 0.82−0.84 e (charge unit), respectively. It is obvious that the overlap populations have the following orders: $(BiO_6)^{9-}$ > $(ZnO_4)^{4-}$ and $(BO_3)^{3-}$ > $(BO_4)^{5-}$. The calculated bond orders of Bi−O, Zn−O, and B−O bonds are 0.19−0.31, 0.18−0.25, and 0.57−0.87 e, respectively (Table S5). Accordingly, we can say that the covalent character of the Bi−O bonds is slightly larger than that of the Zn−O bonds (covalent single-bond order is generally 1.0 e).

The crystal structure of BZB consists of $(BiO_6)^{9-}$, $(B_2O_5)^{4-}$, $(ZnO_4)^{4-}$, and $(B_2O_7)^{8-}$ groups. The B−O, Bi−O, and Zn−O bonding interactions are dominantly covalent in character. Moreover, there is substantial charge density distributed between Bi, Zn, B atoms and O atoms in the $(BiO_6)^{9-}$, $(B_2O_5)^{4-}$, $(ZnO_4)^{4-}$, and $(B_2O_7)^{8-}$ groups. To substantiate the presence of covalent bonding, it can be seen that the charges are nonspherical distributed at the Bi, Zn, B, and O atoms (Figure S5), which are characteristic of systems having covalent interactions.

In previous studies, the origin of the large NLO effect of BIBO mainly comes from the strongly distorted tetragonal $(BiO_4)^{5-}$ groups (almost 90% of the total value).[4,17,38−45] It should be noted that the distorted $(BiO_4)^{5-}$ polyhedra in BIBO originate from heterogeneity of the electronic distribution, that is, second-order Jahn−Teller (SOJT) effect in chemistry.[46,47] To visualize the stereochemically active lone pair (SCALP) of

dx.doi.org/10.1021/jp4013448 | J. Phys. Chem. C 2013, 117, 14149−14157

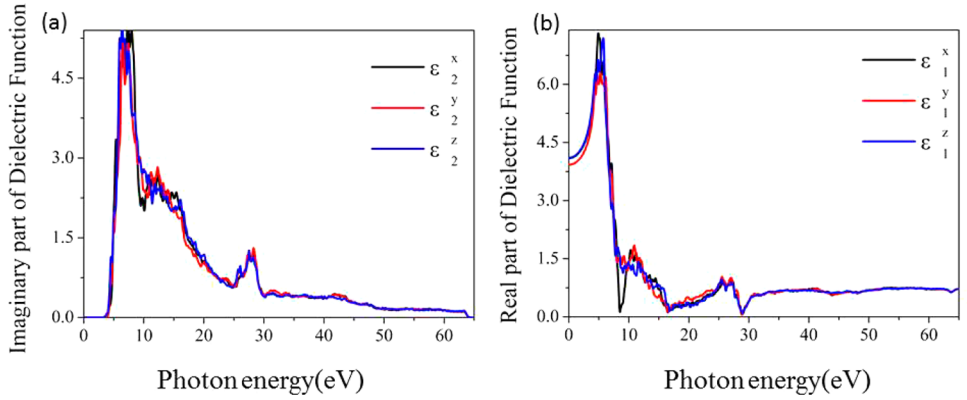

Figure 5. The calculated imaginary parts (a) and real parts (b) of frequency-dependent dielectric functions along three principal dielectric axes of BZB.

Bi^{3+}, we give the ELF map containing the Bi atoms. Figure 3 well describes the polarization and clearly reveals highly asymmetric lobes on the Bi^{3+} cations. These asymmetric lobes may be thought as SCALP. Considering the direction and packing mode of the SCALP in the crystal, there is a superposition of electronic distribution from the lone pairs of Bi1 and Bi2 atoms. The ELF maps along the direction of (100) and (001) for BZB are also given (Figures S6 and S7). These results clearly show that the characteristic of SCALP of Bi^{3+} leads to a heterogeneity electronic distribution in BZB crystal structure. Therefore, this effect may contribute to the overall NLO effect of BZB.

C. Band Structure and Density of States of BZB. The calculated energy bands along the line of high symmetry points in the BZ are illustrated in Figure 4a. The total density of states (DOS) and partial densities of states (PDOS) projected on the constituent atoms in BZB crystal are shown in Figure 4b, which focuses on the electronic states close to the energy band gap. It is found that an indirect LDA band gap of 3.341 eV expands from the valence band (VB) maximum located at G point and the conduction band (CB) minimum located at *Z* point, and is consistent with the experimental band gap of 3.444 eV (Table S6).

We are able to identify the origin of the various groups from the PDOS. For BZB, the bands above the Fermi level are mainly derived from Bi-6p states with small contributions of Zn-4p, B-2p, O-2p states. The lowest valence band group ranging from −23 to −16.7 eV arises mostly from Bi-5d and O-2s states with a slight admixture of B-2s, B-2p states. The middle valence band group between −10.5 and −7.5 eV has significant contributions from Bi-6s and very small contributions from O-2p, B-2s, and B-2p states. However, the bands just below the Fermi level are mostly composed of O-2p states and less mixed Bi-6s and Bi-6p states. The charge transfers across the band gap edge are contributions from the O-2p state to the B-2p, Bi-6p, and Zn-4s states in Figure 4b. By analyzing the PDOS, we note that the Bi−O interactions are dominant at the bottom of the conduction band and also contribute considerably below the Fermi level. It is shown that the highest occupied states should contain the majority of O-2p states and less mixed Bi-6s and -6p states. Such character is intimately related to the lone-pair distortion resulting from the presence of mixing among Bi-6s, 6p states and O-2p states.[35] This could be a major reason why BZB has a narrower band gap as compared to other borate NLO crystals.

D. Linear and NLO Properties of BZB. Because BZB crystallizes in *mm*2 point group, the dielectric functions in three directions (ε^x,ε^y,ε^z) are nonzero. It is noted that the calculation of optical properties was scissor corrected by the difference between the calculated and measured energy gaps, 0.103 eV. The real part of $\varepsilon(\omega)$ in the limit of infinite wavelength is equal to the square of the refractive index *n*. The calculated imaginary parts and real parts of frequency-dependent dielectric functions along three principal dielectric axes of BZB are illustrated in Figure 5. The result shows obvious anisotropy along different dielectric axis directions. The static dielectric constant $\varepsilon_1(\omega = 0)$ represents the dielectric response to the static electric field, and the corresponding $\varepsilon_1^x(0)$, $\varepsilon_1^y(0)$, and $\varepsilon_1^z(0)$ are 3.921, 4.024, and 4.195, respectively.

All of the frequency-dependent optical properties, such as refractive index $n(\omega)$, absorption coefficient $I(\omega)$, reflectivity $R(\omega)$, and electron loss spectrum $L(\omega)$, can be deduced from $\varepsilon_1(\omega)$ and $\varepsilon_2(\omega)$ shown in Figure S8. The dispersion curves of calculated refractive indices also display obvious anisotropy, and indicate an order of $n^x < n^y < n^z$ in the low energy range (Figure S8(a)). Figure 6 shows the calculated and experimental dispersion curves of refractive indices of the BZB crystal. Assignment of dielectric and crystallographic axes is *X*, *Y*, *Z* → *b*, *c*, *a*. The birefringence can be calculated from the linear response functions from which the anisotropy of the index of refraction is obtained. One can see the birefringence Δn in

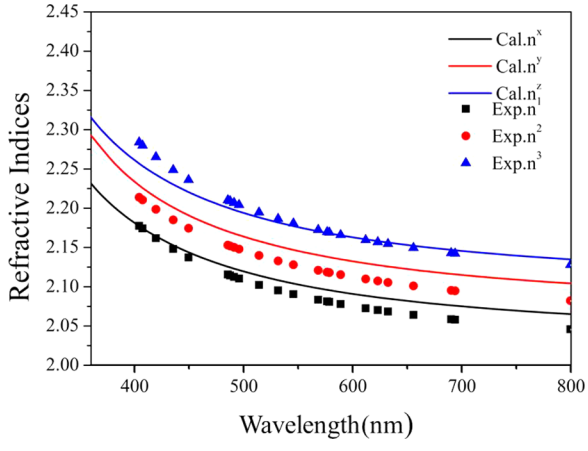

Figure 6. Calculated and experimental dispersion curves of refractive indices of BZB.

dx.doi.org/10.1021/jp4013448 | J. Phys. Chem. C 2013, 117, 14149−14157

Figure 6, which is defined as $n^z - n^x$, is about 0.0685−0.0797 in 1064−404 nm. Generally, BZB has a moderate birefringence Δn and could better fulfill the phase-matching conditions in SHG and optical parametric oscillator.[48−50]

We calculated the second-order coefficients d_{ij} under the static limit within the length gauge. The calculated tensor components d_{31}, d_{32}, and d_{33} are −0.427, 2.721, and −2.585 pm/V, respectively. These calculated absolute coefficients d_{ij} agree basically with experimental ones, which proves the validity of our studies on BZB with the LDA plane-wave pseudopotential method.

E. Origin of the SHG. The practical no-divergent formalism for evaluating NLO properties for solids was proposed by Sipe et al.[51] and further rearranged by Rashkeev[52] and later improved by Lin et al.[17] Apart from the remarkable breakthrough of making calculation possible, the use of a sum-over-states formalism has the advantage of providing a natural way to see the total quantities as contribution from various parts.[53] This sum-over-states type formalism is explicitly expressed with terms having momentum matrix elements in the numerator and energy eigenvalue difference in the denominator. In the past decade, a theoretical method called "real-space atom-cutting method" has been used to analyze the linear refractive indices and SHG coefficients of various NLO crystals such as BBO,[17] LBO,[38] BIBO,[42] KDP,[43] and $BaAlBO_3F_2$,[49] with great success.

The real-space atom-cutting method was employed by cutting all ions except A from the original wave functions $\chi^n(A) = \chi^n$ (all ions except A are cut). $\chi^n(A)$ is denoted as the contribution of ion A to the nth-order polarizability. The method divides the real space into individual zones, each of which contains an ion. Subsequently, we set the band wave function to zero in the zones that belong to a specific ion or a cluster, which is referred to as "cutting", when the contribution of the ion or cluster is believed to be cut away.[36] Therefore, when the ions are cut from the total wave functions, the contribution of the ions is extracted from the total wave functions. Furthermore, various manners of cutting can result in various contributions of transitions; for example, we can find the contribution of transitions from a Bi atomic orbital in the valence bands to the O atomic orbital in conduction bands to the optical properties of BiO_6 by cutting O wave functions from valence bands and cutting Bi wave functions from the conduction bands.

For analyzing the optical response of BZB, we have to determine the suitable cutting radius of Bi, Zn, B, and O.[13] The charge is transferred in Bi, Zn, B, and O atoms, and the charge density in the B−O group is relatively local as compared to that of the Bi−O, Zn−O groups (Figures S5−S7). The nonspherical symmetric distribution of Bi, Zn, B, and O atoms indicates that these atoms can effectively overlap and form covalent bonds. The cutting radius of Bi is 1.50 Å by investigating the charge-density distribution between the nearest Bi and O ions. Following the rule of keeping the cutting spheres of Bi and O in contact and not overlapped, the cutting radius of O is set to 1.11 Å. Finally, the covalent radius 0.88 Å of B is chosen as its cutting radius, and the cutting radius of Zn is set as 1.25 Å. Furthermore, the density of the SHG effect for BZB was calculated to clarify further the validity of the cutting pattern.[53,54] From the density of the SHG effect in Figure 7, the density distribution indicates that there is a nonspherical distribution around the Bi^{3+} ion with an apparent electron density overlap between bismuth, zinc, or boron and oxygen

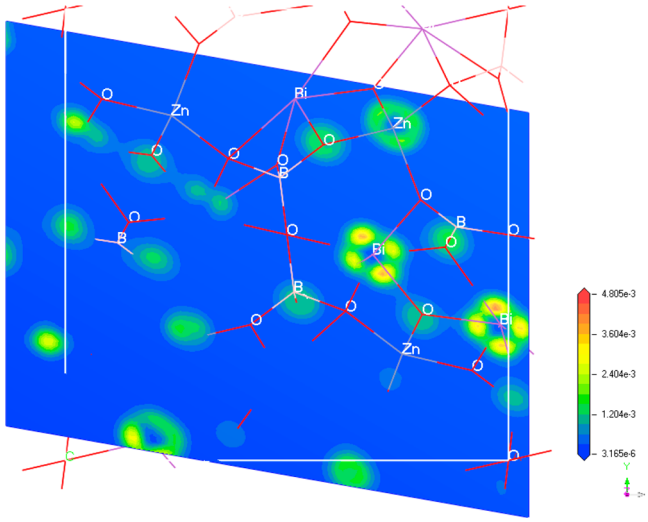

Figure 7. The density of the SHG effect in $(BiO_6)^{9-}$ group perspective shadow along z axes of BZB.

atoms. The overlap behaviors in the density distribution confirm that choosing the $(BiO_6)^{9-}$, $(B_2O_5)^{4-}$, $(ZnO_4)^{4-}$, and $(B_2O_7)^{8-}$ groups as the NLO active group is feasible to explore the contributions to the SHG effects.

In Table 1, the calculated refractive indices, birefringence, and SHG coefficient using the atom-cutting analysis are reported in comparison with the corresponding experimental and calculated results at 1064 nm, respectively. The following conclusions are obtained: (1) It is shown that the contribution of the $(BiO_6)^{9-}$ group to the refractive indices is comparable to that of the $(B_2O_5)^{4-}$, $(ZnO_4)^{4-}$, and $(B_2O_7)^{8-}$ groups, whereas its contribution to the birefringence can be neglected. The contribution of $(BiO_6)^{9-}$ to the birefringence is only about 5.59%, the contributions of $(ZnO_4)^{4-}$ and $(B_2O_7)^{8-}$ anionic groups are about 31.47%, 25.96%, and $(B_2O_5)^{4-}$ anionic groups contribute more than 36.98% to the anisotropy of refractive indices. For the birefringence of BZB, the relationships of the contribution are $(B_2O_5)^{4-} > (ZnO_4)^{4-} > (B_2O_7)^{8-} > (BiO_6)^{9-}$. (2) From the decomposed d_{31} and d_{33} coefficients, the contributions from the $(BiO_6)^{9-}$ group are about 98.20% and 66.59% to the overall SHG coefficient, which are significant larger than other groups in BZB. However, the contributions from the $(B_2O_5)^{4-}$ and $(BiO_6)^{9-}$ groups are comparable from the result of decomposed d_{32} coefficients. The contributions of $(B_2O_7)^{8-}$ and $(ZnO_4)^{4-}$ to the overall SHG coefficient are relatively small, while the contributions from these two groups to the anisotropy of refractive indices cannot be neglected. Moreover, the sum of the contributions from individual groups in the crystal is larger than the original calculated value of the whole crystal due to the repeated calculation of the wave functions of some shared oxygen atoms. In other words, the orbitals on the oxygen atoms linked with the neighbor anionic groups are used twice in the real-space atom-cutting procedures. Inversely, if there are no shared oxygen atoms between the individual groups, the calculated SHG coefficient will be nearly the same as the result of the sum of contributions from individual groups. A typical case happens in $KBe_2BO_3F_2$ that no shared atoms exist between BeO_3F and BO_3 groups.[55]

To further improve the understanding of the origin of SHG, the band-resolved method has been used to analyze the contribution of the BZB crystal electronic subsystem.[17,53] A sum-over-states type formula is used for the evaluation of static

dx.doi.org/10.1021/jp4013448 | J. Phys. Chem. C 2013, 117, 14149−14157

Table 1. Comparison of the Calculated and the Experimental Values of Refractive Indices, Birefringence, and SHG Coefficient, Together with Atom-Cutting Analysis Results for BZB Crystal

	n^x	n^y	n^z	Δn	d_{31} (pm/V)	d_{32} (pm/V)	d_{33} (pm/V)
BiO_6	1.12707	1.12812	1.13543	0.0073	−0.3620	1.1360	−2.1956
ZnO_4	1.87282	1.89934	1.91395	0.0411	0.1820	0.1270	−1.7880
B_2O_5	1.87093	1.89909	1.94734	0.0483	−0.0949	1.4860	−1.0283
B_2O_7	1.83344	1.86736	1.88312	0.0339	−0.0937	1.0563	1.7148
sum				0.1306	−0.3686	3.8053	−3.2971
exp	2.05197	2.06454	2.10817	0.0787	0.9109	3.0828	1.0149
calcd	2.05197	2.09001	2.12054	0.0685	−0.4270	2.7210	−2.5850

SHG coefficients. The orbital contribution to $\chi^{(2)}$ can be decomposed on an energy level-by-level basis by partially summing only two out of all three band indices. On the basis of band-resolved, the dominant orbitals that give major contribution to a SHG process can be identified and analyzed.[52] The interband transitions from a $(B_2O_5)^{4-}$ group states in the VB to a $(BiO_6)^{9-}$ group states in the CB are the dominant source of large d_{32}, because the total contribution of all processes including such transitions is 1.486 pm/V, which is 54.61% of the total d_{32} calculated values. In addition, the respective influence of the various transitions on the optical responses is elaborated. The contributions of different transitions to SHG effect are calculated (Table 2). The contributions of the virtual electron (VE) process to the SHG effect are 96.55%, 96.48%, and 99.65% for d_{31}, d_{32}, and d_{33}.

Table 2. Contributions of SHG Coefficients of Different Transitions for BZB Crystal

	d_{31} (pm/V)	d_{32} (pm/V)	d_{33} (pm/V)
BZB	−0.4270	2.7210	−2.5850
contributions			
VE	−0.4080	2. 6252	−2.5761
VH	−0.0190	0.0958	−0.0089
TB	0.0000	0.0000	0.0000

The structural factors and the density of the SHG effect in Figure 7 lead us to choose the $(BiO_6)^{9-}$ group as a NLO active group to calculate its contributions to the SHG effects. However, if only the Bi^{3+} cations are chosen, the results of the contribution to the SHG coefficients are much less than those of the $(BiO_6)^{9-}$ groups (for example, $d_{31}^{\text{only Bi}} = -0.188$ pm/V, $d_{32}^{\text{only Bi}} = -0.128$ pm/V, $d_{33}^{\text{only Bi}} = 0.396$ pm/V). This implies that the electronic transfer between Bi and O in the $(BiO_6)^{9-}$ group is one of the reasons for producing relative larger SHG coefficients for BZB crystal. In addition, the detailed structural analysis (see Figure S2(c) and Table S2) shows that the $(BiO_6)^{9-}$ group is a heavily deformed octahedron; the angles formed by the vertex oxygen, central bismuth, and base oxygen inside vary from 57.24° to 152.6°, far from 90° in a regular octahedron. In fact, the NLO crystals containing deformed MO_6 octahedra usually have very large SHG coefficients, as in the cases of $LiNbO_3$, $KNbO_3$, $BaTiO_3$, etc.[56] Moreover, in the structure of BZB, two $(BO_3)^{3+}$ triangles condense into a $(B_2O_5)^{4-}$ group, and they are not in the same plane. The angles of the O−B−O bonds are found to be 116.8°, 175.5°, and 125.6°, respectively. Consequently, the $(BO_3)^{3-}$ or $(B_2O_5)^{4-}$ group is one but not the only one reason inducing the large NLO effects. As described above, the main sources of the SHG properties of BZB are cooperation from the distorted $(BiO_6)^{9-}$ and $(B_2O_5)^{4-}$ groups. This result is in accordance with other materials such as BIBO (see Table S7).[42]

CONCLUSION

In summary, the linear and NLO properties for BZB were studied experimentally and theoretically. A large BZB single crystal has been successfully grown by the Czochralski method. The absorption edge of BZB is 360 nm measured from the optical transmittance spectrum, and consequently its experimental band gap is 3.444 eV, which is well consistent with the electronic band structure studies that BZB is an indirect gap material with the value of 3.341 eV. The refractive indices were measured by the minimum-deviation method. The birefringence is about 0.0787−0.1064 around 1064−404 nm. The calculated birefringence is about 0.0685−0.0797 from 1064 to 404 nm. The SHG coefficients of BZB were measured via the standard Maker fringe method, with the results as follows: $|d_{31}| = 0.911$ pm/V, $|d_{32}| = 3.083$ pm/V, and $|d_{33}| = 1.015$ pm/V, and the calculated NLO coefficients are $d_{31} = -0.427$ pm/V, $d_{32} = 2.721$ pm/V, and $d_{33} = -2.585$ pm/V, which agree basically with the measured ones.

We have presented a further investigation on the electronic structure, electronic charge density, ELF and Mulliken population analyses, and optical properties analyses of the BZB via first-principles methods. Careful comparison of the charge density and ELF results indicates that the B−O, Bi−O, and Zn−O are mainly covalent interactions. In addition, the contributions of different types of transitions to certain optical properties, including dielectric function, refractive indices, birefringence, and static SHG coefficients, have been calculated. It is shown that the linear optical properties have a strong anisotropy and large birefringence. For the NLO properties, BZB has a wide SHG phase-matching range, and the large NLO coefficients further suggest that it is a promising NLO material.

Meanwhile, the respective contributions of different groups to the overall optical properties have been investigated by the real-space atom-cutting method. It is shown that the contributions of $(BiO_6)^{9-}$ groups to the birefringence are very small and can be neglected, and the contributions of $(ZnO_4)^{4-}$, $(B_2O_5)^{4-}$, and $(B_2O_7)^{8-}$ anionic groups to the birefringence are dominant and comparable. The results also indicate that the exceptionally large d_{ij} coefficients of BZB crystal mainly come from the contribution of the $(BiO_6)^{9-}$ and $(B_2O_5)^{4-}$ groups. The comprehensive understanding of the microscopic mechanism of optical effects in BZB is important to elucidate its structure−property relationship and provides a general strategy for searching new NLO materials.

dx.doi.org/10.1021/jp4013448 | J. Phys. Chem. C 2013, 117, 14149−14157

■ ASSOCIATED CONTENT

Supporting Information

An X-ray crystallographic file (CIF); crystal data and structure refinement; XRD patterns; selected bond lengths (Å) and angles (deg); the optimized atomic positions and lattice parameters between experimental and theoretical results; calculated bond orders; calculated band structures; total and partial density of states and state energies of the H-VB and the L-CB at the same k-point; the experimental values of refractive indices; assignment of dielectric and crystallographic axis; the Bi^{3+} lone pair map of electronic local function viewed down the Z and X axes; calculated charge density in the (010) plane; the calculated frequency-dependent refractive indices n (ω) (a), reflectivity spectra R (ω) (b), absorption coefficient I (ω) (c), and loss function L (ω) (d) along three principal dielectric axes; comparison of the analyses of birefringence and SHG coefficients of origins with the other two NLO crystals; and calculated and experimental interatomic distances of the relative deviation of the Bi−O for BZB. This material is available free of charge via the Internet at http://pubs.acs.org.

■ AUTHOR INFORMATION

Corresponding Author

*Phone: (86)991-3859931. Fax: (86)991-3838957. E-mail: zhyang@ms.xjb.ac.cn (Z.Y.); slpan@ms.xjb.ac.cn (S.P.).

Notes

The authors declare no competing financial interest.

■ ACKNOWLEDGMENTS

This work is supported by the "Western Light Joint Scholar Foundation" Program of Chinese Academy of Sciences (Grant no. LHXZ201101), the "National Natural Science Foundation of China" (Grant nos. 11104344, U1129301, 51172277, 21101168), the National Key Basic Research Program of China (Grant no. 2012CB626803), the Main Direction Program of Knowledge Innovation of Chinese Academy of Sciences (Grant no. KJCX2-EW-H03-03), the "One Hundred Talents Project Foundation Program" of the Chinese Academy of Sciences, the National "One Thousand Youth Talents Project Foundation Program" (The Recruitment Program of Xinjiang Special Program on Global Experts for Young Scholar), Major Program of Xinjiang Uygur Autonomous Region of China during the 12th Five-Year Plan Period (Grant no. 201130111), and the "High Technology Research and Development Program" of Xinjiang Uygur Autonomous Region of China (Grant no. 201116143).

■ REFERENCES

(1) Lines, M. E.; Glass, A. M. *Principles and Applications of Ferroelectrics and Related Materials*; Oxford University Press: Oxford, 1991; p 576.
(2) Becker, P. *Adv. Mater.* **1998**, *10*, 979.
(3) Mori, Y.; Kuroda, I.; Nakajima, S.; Sasaki, T.; Nakai, S. *Appl. Phys. Lett.* **1995**, *67*, 1818.
(4) Chen, C. T.; Wu, B. C.; Jiang, A.; You, G. *Sci. Sin., Ser. B* **1985**, *28*, 235.
(5) Ok, K. M.; Chi, E. O.; Halasyamani, P. S. *Chem. Soc. Rev.* **2006**, *35*, 710.
(6) Barbier, J.; Penin, N.; Cranswick, L. M. *Chem. Mater.* **2005**, *17*, 3130.
(7) Barbier, J.; Penin, N.; Cranswick, L. M. *Solid State Sci.* **2005**, *7*, 1055.
(8) Li, F.; Hou, X. L.; Pan, S. L.; Wang, X. A. *Chem. Mater.* **2009**, *21*, 2846.
(9) Li, F.; Pan, S. L.; Hou, X. L.; Yao, J. *Cryst. Growth Des.* **2009**, *9*, 4091.
(10) Li, F.; Pan, S. L.; Hou, X. L.; Zhou, Yao, J. Z. *J. Cryst. Growth* **2010**, *312*, 2383.
(11) Li, F.; Pan, S. L. *J. Cryst. Growth* **2011**, *318*, 629.
(12) Reshak, A. H.; Chen, X. A.; Kityk, I. V.; Auluck, S. *Curr. Opin. Solid State Mater. Sci.* **2007**, *11*, 33.
(13) Reshak, A. H.; Chen, X. A.; Kityk, I. V.; Auluck, S.; Iliopoulos, K.; Couris, S.; Khenata, R. *Curr. Opin. Solid State Mater. Sci.* **2008**, *12*, 26.
(14) Becker, P.; Liebertz, J.; Bohatý, L. *J. Cryst. Growth* **1999**, *203*, 149.
(15) Chen, C. T.; Wu, Y. C.; Jiang, A. D.; Wu, B. C.; You, G. M.; Li, R. K.; Lin, Z. S. *J. Opt. Soc. Am. B: Opt. Phys.* **1989**, *6*, 616.
(16) Chen, C. T.; Wang, Y.; Xia, Y.; Wu, B.; Tang, D.; Wu, K.; Wen, Z.; Yu, L.; Mei, L. *J. Appl. Phys.* **1995**, *77*, 2268.
(17) Lin, J.; Lee, M. H.; Liu, Z. P.; Chen, C. T.; Pickard, C. J. *Phys. Rev. B* **1999**, *60*, 51.
(18) Rashkeev, S. N.; Lambrecht, W. R. L.; Segall, B. *Phys. Rev. B* **1998**, *57*, 3905.
(19) Francis, G. P. *J. Phys.: Condens. Matter* **1990**, *2*, 4395.
(20) Milman, V.; Lee, M. H.; Payne, M. C. *Phys. Rev. B* **1994**, *49*, 16300.
(21) Payne, M. C.; Teter, M. P.; Allan, D. C.; Arias, T. A.; Joannopoulos, J. D. *Rev. Mod. Phys.* **1992**, *64*, 1045.
(22) Clark, S. J.; Segall, M. D.; Pickard, C. J.; Hasnip, P. J.; Probert, M. J.; Refson, K.; Payne, M. C. *Z. Kristallogr.* **2005**, *220*, 567.
(23) Lee, M. H.; Lin, J. S.; Payne, M. C.; Heine, V.; Milman, V. *Psi-k Newsletters* **2005**, *67*, Highlight, http://www.psi-k.org/newsletters/News_67/Highlight_67.pdf.
(24) Rappe, A. M.; Rabe, K.; Kaxiras, M. E. *Phys. Rev. B* **1990**, *41*, 1227.
(25) Lee, M. H. PhD Thesis, Cambridge University, 1996.
(26) Lin, J. S.; Qteish, A.; Payne, M. C.; Heine, V. *Phys. Rev. B* **1993**, *47*, 4174.
(27) Monkhorst, H. J.; Pack, J. D. *Phys. Rev. B* **1976**, *13*, 5188.
(28) Perdew, J. P.; Wang, Y. *Phys. Rev. B* **1992**, *45*, 13244.
(29) Godby, R. W.; Schluter, M.; Sham, L. J. *Phys. Rev. B* **1988**, *37*, 10159.
(30) Wang, C. S.; Klein, B. M. *Phys. Rev. B* **1981**, *24*, 3417. Hybertsen, M. S.; Louie, S. G. *Phys. Rev. B* **1986**, *24*, 5390.
(31) Levine, Z. H.; Allan, D. C. *Phys. Rev. B* **1991**, *43*, 4187.
(32) Hughes, J. L. P.; Sipe, J. E. *Phys. Rev. B* **1996**, *53*, 10751.
(33) Godby, R. W.; Schlueter, M.; Sham, L. J. *Phys. Rev. B* **1988**, *37*, 10159.
(34) Gunnarsson, O.; Schoenhammer, K. *Phys. Rev. Lett.* **1986**, *56*, 1968.
(35) Bassani, F.; Parravicini, G. P. *Electronic States and Optical Transitions In Solids*; Pergamon Press Ltd.: Oxford, 1975; p 149.
(36) Yang , B. P.; Hu, C. L.; Xu, X.; Sun, C. F.; Zhang, J. H.; Mao, J. G. *Chem. Mater.* **2010**, *22*, 1545.
(37) Palik, E. D. *Handbook of Optical Constants of Solids*; Academic Press: New York, 1985.
(38) Lin, Z. S.; Lin, J.; Wang, Z. Z.; Chen, C. T.; Lee, M. H. *Phys. Rev. B* **2000**, *62*, 1757.
(39) Lin, Z. S.; Kang, L.; Zheng, T.; He, R.; Huang, H.; Chen, C. T. *Comput. Mater. Sci.* **2012**, *60*, 99.
(40) Lin, Z. S.; Wang, Z. Z.; Chen, C. T.; Chen, S. K.; Lee, M. H. *Chem. Phys. Lett.* **2003**, *367*, 523.
(41) Lin, Z. S.; Wang, Z. Z.; Chen, C. T.; Chen, S. K.; Lee, M. H. *J. Appl. Phys.* **2003**, *93*, 9717.
(42) Lin, Z. S.; Wang, Z. Z.; Chen, C. T.; Lee, M. H. *J. Appl. Phys.* **2001**, *9*, 5585.
(43) Lin, Z. S.; Wang, Z. Z.; Chen, C. T.; Lee, M. H. *Chem. Phys.* **2003**, *118*, 2349.
(44) Huang, H.; Lin, Z. S.; Bai, L.; Hu, Z. G.; Chen, C. T. *J. Appl. Phys.* **2009**, *106*, 103107.

(45) Fabris, S.; de Gironcoli, S.; Baroni, S.; Vicario, G.; Balducci, G. *Phys. Rev. B* **2005**, *71*, 041102.
(46) Ra, H. S.; Ok, K. M.; Halasyamani, P. S. *J. Am. Chem. Soc.* **2003**, *125*, 7764.
(47) Chang, H. Y.; Kim, S. H.; Ok, K. M.; Halasyamani, P. S. *J. Am. Chem. Soc.* **2009**, *131*, 6865.
(48) Glimsdal, E.; Carlsson, M.; Eliasson, B.; Lindgren, M.; Minaev, B. *J. Phys. Chem. A* **2007**, *111*, 244.
(49) Reshak, A. H.; Stys, D.; Auluck, S.; Kityk, I. V. *Phys. Chem. Chem. Phys.* **2011**, *13*, 2945.
(50) Reshak, A. H.; Ortiz, D. A. O. *J. Phys. Chem. B* **2009**, *113*, 13208.
(51) Aversa, C.; Sipe, J. E. *Phys. Rev. B* **1995**, *52*, 14636. Ghahramani, E.; Moss, D. J.; Sipe, J. E. *Phys. Rev. B* **1991**, *43*, 8990.
(52) Rashkeev, S. N.; Lambrecht, W. R. L. *Phys. Rev. B* **2001**, *63*, 165212.
(53) Lee, M. H.; Yang, C. H.; Jan, J. H. *Phys. Rev. B* **2004**, *70*, 235110.
(54) Lo, C. H.; Lee, M. H. The Role of Electron Lone-pair in the Optical Nonlinearity of Oxide, Nitride and Halide Crystals. Master Thesis, Taiwan, 2005; p *29*.
(55) Chen, C. T.; Ye, N.; Lin, J.; Jiang, J.; Zeng, W. R.; Wu, B. C. *Adv. Mater.* **1999**, *11*, 1071.
(56) Chen, C. T. Development of New NLO Crystals in the Borate Series. In *Laser Science and Technology, an International Handbook*; Letokhov, V. S., Shank, C. V., Shen, Y. R., Walther, H., Eds.; Harwood: Chur, Switzerland, 1993; Vol. *15*, Chapter 1.